International Journal of Structural Integrity

A data-driven hybrid method combining experiments, finite element modeling and machine learning for impact response prediction of TPU composites

Received 21 July 2025
Revised 2 October 2025
Accepted 4 October 2025

Shunqi Zhang, Luca Lomazzi, Dayou Ma and Andrea Manes
Department of Mechanical Engineering, Politecnico di Milano, Milan, Italy

Abstract

Purpose – This study aims to develop a robust and generalizable hybrid strategy for investigating impact behaviors of high-performance composites, significantly advancing composite impact engineering and demonstrating strong potential for applications in protective and structural systems.

Design/methodology/approach – With the hybrid framework that integrates experimental testing, finite element (FE) modeling and machine learning (ML), the study on the low-velocity impact behavior of Kevlar fiber-reinforced composites with thermoplastic polyurethane matrix was carried out: with the validation of the FE model by experiments, the numerical model was used to produce data to train the ML methods.

Findings – The best-performing Levenberg–Marquardt artificial neural network model achieved excellent agreement with FE simulation data, yielding a correlation coefficient $R > 0.98$ and a low mean squared error, which was also proven through experimental validation with satisfactory accuracy.

Originality/value – In the current work, the combined method with the FE model, experiments and ML was developed for low-velocity impact of thermoplastic composite materials. The damage process was investigated, while the accuracy of the proposed methodology was verified when compared to experimental outcomes.

Keywords Thermoplastic polyurethane, Soft-matrix composite, Low-velocity impact, Data-driven method, Levenberg–Marquardt algorithm

Paper type Research article

1. Introduction

Composite materials are widely adopted in advanced structural applications owing to their excellent stiffness-to-weight ratios, resistance to corrosion and fatigue and the tailorability of mechanical response (Yakin *et al*., 2025; Senol *et al*., 2025a, b). Accordingly, their response to impact loading is a pivotal consideration in design and safety assessments (Siengchin, 2023; Karsandik *et al*., 2023). Fiber-reinforced composites conventionally adopt thermoset polymer matrices like epoxies, which deliver high stiffness and strength, albeit at the expense of limited fracture toughness (Rezasefat *et al*., 2022a; Staroverov *et al*., 2022). Thermoplastic composites have gained increasing attention as a promising alternative, offering improved manufacturing flexibility, enhanced damage tolerance and excellent mechanical stability under extreme service conditions (Boria *et al*., 2017; Yildirim *et al*., 2025; Kurdiş *et al*., 2025; Şenyurt *et al*., 2025). The inherent ductility and deformation capacity of thermoplastics can facilitate composites' superior delamination resistance and energy absorption capabilities (Sun *et al*., 2018). Recent investigations have been conducted on characterizing the mechanical behavior and failure mechanisms of thermoplastic matrix composites under impact conditions (Hazzard *et al*., 2017). For instance, Shah *et al*. (2021) demonstrated that

© Shunqi Zhang, Luca Lomazzi, Dayou Ma and Andrea Manes. Published by Emerald Publishing Limited. This article is published under the Creative Commons Attribution (CC BY 4.0) license. Anyone may reproduce, distribute, translate and create derivative works of this article (for both commercial and non-commercial purposes), subject to full attribution to the original publication and authors. The full terms of this license may be seen at Link to the terms of the CC BY 4.0 licence

International Journal of Structural Integrity
Emerald Publishing Limited
e-ISSN: 1757-9872
p-ISSN: 1757-9864
DOI 10.1108/IJSI-07-2025-0180

Downloaded from http://www.emerald.com/ijsi/article-pdf/doi/10.1108/IJSI-07-2025-0180/10416281/ijsi-07-2025-0180en.pdf by Politecnico di Milano user on 06 March 2026

glass-fiber-reinforced thermoplastic acrylic composites exhibited higher damage initiation thresholds compared to their thermoset counterparts. Liu *et al.* (2021) found that plastic deformation is one of the primary energy dissipation mechanisms during impacts on thermoplastic polyethylene composites. Thermoplastic polyurethane (TPU) – also broadly known as thermoplastic elastomers, a relatively recent development among thermoplastics – features a microphase-separated architecture comprising alternating soft and hard segments, resulting in an exceptional combination of elasticity, strength and impact resilience surpassing that of conventional epoxies (Miller *et al.*, 2015). Growing evidence supports the superior impact resistance of TPU composites (Lin *et al.*, 2023; Montazeri *et al.*, 2025a, b). Applying TPU either as a surface coating or as electrospun interleaves redistributes impact energy, suppresses delamination and improves post-impact performance (Rizzo *et al.*, 2020; Lu *et al.*, 2025). Russo *et al.* (2016) reported no delamination in TPU glass-fiber laminates following low-velocity impacts at ambient and sub-zero temperatures. In the carbon fiber (CF) system, Pechlivani (2024) validated the improved mechanical response and flexural performance of 3D-printed TPU/CF composites under Quasi-static tests. Although current findings underscore the promise of TPU composite systems for impact mitigation, further in-depth exploration and advanced methodologies are essential to fully harness their mechanical potential.

Traditional methodologies for evaluating composite impact behavior integrate experimental testing with numerical modeling, addressing a wealth of literature (Paolo *et al.*, 2011; Boukar *et al.*, 2022; Han *et al.*, 2024). Explicit finite element (FE) tools such as Livermore Software DYNA (LS-DYNA) and Abaqus are widely employed for simulating impact phenomena in composites due to their capacity to capture complex damage modes and facilitate parameter calibration to align with experimental observations (Zhang *et al.*, 2025a; Kumar *et al.*, 2024). For example, Boria *et al.* (2015) performed both experimental and numerical investigations on carbon and/or epoxy composites and demonstrated that, although requiring higher computational cost compared to shell-element models, solid-element FE models using the MAT 55 card in LS-DYNA yielded higher fidelity in predicting intra- and inter-laminar damage. Nevertheless, relying solely on FE simulations becomes computationally prohibitive when examining multivariate parameter spaces. To overcome this limitation, alternative methods have been proposed to augment conventional techniques. Machine learning (ML) has increasingly been integrated into composite mechanics, offering promising outcomes in impact-related scenarios (Sorour *et al.*, 2024; Hasebe *et al.*, 2025; Qiu *et al.*, 2022). Among ML techniques, artificial neural networks (ANNs) have emerged as robust tools for modeling the mechanical response of composite materials (Ding *et al.*, 2022). Feed-forward neural networks, in particular, have shown strong predictive capabilities for composite behavior under diverse loading conditions (Xiong *et al.*, 2023; Zhang *et al.*, 2025b). Zhang *et al.* (2025b) developed an ANN capable of predicting impact force histories of composite laminates with a high correlation coefficient of 0.98. Mezeix *et al.* (2023) reported that their neural network effectively detected delamination and estimated damage-related parameters with error rates below 10%. Once trained, ANN models provide near-instantaneous predictions, enabling real-time analysis and high-throughput evaluation, which are unattainable with conventional FE simulations.

However, a key challenge in employing ANNs lies in the need for large, diverse and high-quality training datasets. Generating such datasets purely through experiments can be prohibitively costly and time-consuming, thereby undermining the efficiency gains of ML. To address this, validated FE models can be used as synthetic data generators, forming the basis of hybrid FE-ML frameworks that combine the strengths of physics-based and data-driven approaches (Lei *et al.*, 2021; Stephen *et al.*, 2022; Pittie *et al.*, 2023). For instance, Stephen *et al.* (2022) utilized simulation-generated datasets to train ANN models that predicted impact responses of various laminate configurations with approximately 6% error. Likewise, Pittie *et al.* (2023) combined experimental calibration with FE simulations to train ANNs capable of predicting back-face deformation and the number of perforated layers. These studies

Downloaded from http://www.emerald.com/ijsi/article-pdf/doi/10.1108/IJSI-07-2025-0180/10416281/ijsi-07-2025-0180en.pdf by Politecnico di Milano user on 06 March 2026

underscore the increasing relevance of ML and FE-ML hybrids in accelerating composite impact analysis and enhancing design processes.

Building on this foundation, we develop a hybrid, data-driven framework to investigate the low-velocity impact response of TPU-matrix Kevlar-fiber composites with emphasis on the effect of matrix content, enabling efficient prediction of the laminate's impact response. The methodology integrates impact experiments, FE modeling and ANNs. Low-velocity impact (LVI) experiments were conducted to establish reliable data, followed by the development of a ply-level macro-homogeneous FE model in LS-DYNA. The numerical model was successfully validated against experimental tests, and the influence of matrix content on impact behavior has been examined. Subsequently, the model was utilized to generate a structured dataset spanning impact energy and TPU content for network training. Alternative network architectures and training algorithms are systematically assessed to learn mappings from inputs to key impact-response metrics. The resulting ANN surrogate delivers accurate, near-instantaneous predictions and exhibits strong agreement with independent unseen experimental measurements, enabling rapid performance evaluation and early-stage design of impact-resistant TPU composites.

2. Material

The reinforcement material employed in this study is Kevlar® XP S307 fabric (305 g/m^2, thickness 0.27 mm, 440 tex), which features two layers of parallel fibers superimposed, stitched together and arranged at $+45^o$ and -45^o orientations. Mantoflex® 2198A TPU was selected as the matrix material. Initially, the TPU material was provided in pellet form with a density of 1.23 g/cm^3, a Shore hardness of 98A and a melt flow rate of 4.5 g/10 min (205 °C, 2.16 kg). Prior to processing, these TPU pellets underwent drying at 105 °C for 5 h using a Fanem 3155E oven. Subsequently, the dried pellets were then processed using an AX Plásticos Lab-16 extruder operated at 140–200 °C and 72 rpm to produce TPU films with an areal density of 60 g/m^2 and an average thickness of 60 μm. An annealing treatment was conducted at 80 °C for 8 h during post-processing to enhance the uniformity of the material's crystalline microstructure.

Previous studies have identified several techniques for integrating thermoplastic matrices with reinforcements, including prepregging (Goodman and Loos, 1990), film calendaring (Ali *et al*., 2003) and aqueous suspension methods (Texier *et al*., 1993). Among these, hot press forming (Al-Dhaheri *et al*., 2024), recognized as one effective process in thermoplastic composite manufacturing, was utilized in this study, and the process cycle is depicted in Figure 1(a). In the current fabrication, hot press forming was conducted using pre-heated metal molds installed on a semi-automated hydraulic press (Carver CMG30H-12-ASTM). The process initiates by arranging laminate layers at 200 °C and 10 MPa pressure. After forming, the laminate is transferred to an oven, where it undergoes curing at 80 °C for 15 h to complete solidification.

Three laminate configurations with different TPU matrix content were fabricated. The stacking sequences and configurations are shown in Figure 1(b), and detailed information are reported in Table 1. For the nomenclature on the sample, the letter "K" denotes the aramid layers and "PU" refers to the TPU film layers. Each laminate configuration consists of eight aramid layers, intercalated by 1, 2 or 3 TPU films. The final laminate productions were sectioned along the thickness direction, and the laminate's cross-sectional views were observed using optical microscopy, which is presented in Figure 1(b). The dark regions correspond to the aramid layers, while the lighter regions represent the TPU matrix. K8_1PU and K8_3PU are considered as the TPU composite with the minimum and maximum matrix capacity. Below the minimum content, insufficient infiltration of TPU into the aramid fabric occurs, while above the maximum content, excessive resin accumulation leads to degraded laminate quality after hot pressing. The K8_2PU configuration provides a middle state between these two extremes. To obtain the fundamental material mechanical properties of the

Downloaded from http://www.emerald.com/ijsi/article-pdf/doi/10.1108/IJSI-07-2025-0180/10416281/ijsi-07-2025-0180en.pdf by Politecnico di Milano user on 06 March 2026

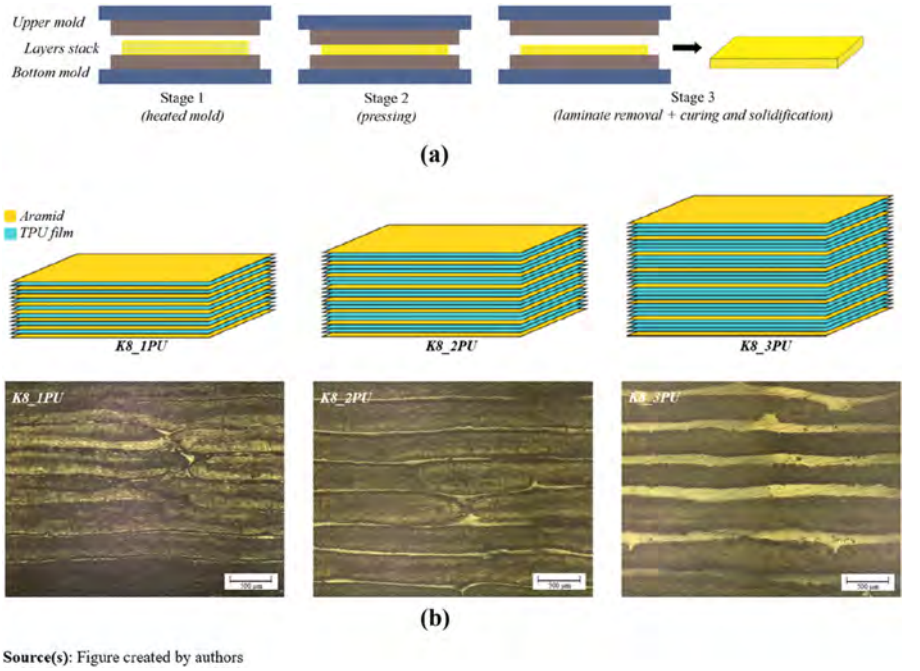

Figure 1. (a) Hot press forming cycle and (b) illustration of the laminate configurations and the optical microscopy images on cross-section

Table 1. Summary of the TPU composite laminates

Laminates	Aramid layers	TPU film layers	Thickness (mm)	Matrix volume fraction
K8_1PU	8	7	2.44	13.9%
K8_2PU		14	2.86	29.9%
K8_3PU		21	3.17	38.1%

Source(s): Table created by authors

specimens, a series of tests adhering to the American Society for Testing and Materials (ASTM) standards were performed as material characterization for the FE models.

3. Methodology

Figure 2 provides a schematic illustration outlining the three-stage hybrid framework adopted in this study. First, Section 3.1 establishes the experimental foundation through low-velocity impact tests to provide reliable observations. Second, Section 3.2 develops a matrix-content-related ply-level FE model in LS-DYNA based on the laminate's design and specimen architecture. After validation, an LS-OPT workflow has been built, which runs in conjunction with the model in LS-DYNA, to generate a structured dataset for the ML. Third, Section 3.3 introduces the Levenberg–Marquardt and scaled conjugate gradient (SCG) algorithms. These algorithms are employed for feed-forward neural network training to identify the optimal network and achieve accurate prediction on impact response. In the end, this hybrid

Downloaded from http://www.emerald.com/ijsi/article-pdf/doi/10.1108/IJSI-07-2025-0180/10416281/ijsi-07-2025-0180en.pdf by Politecnico di Milano user on 06 March 2026

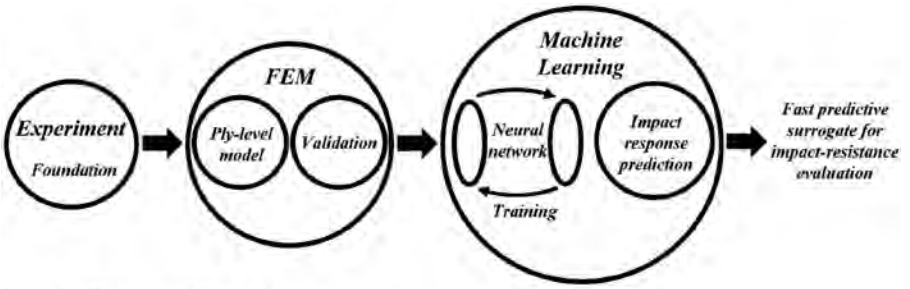

Source(s): Figure created by authors

Figure 2. Scheme of the proposed hybrid experiment-FE modeling-machine learning methodology for impact response prediction of TPU composites

methodology establishes an efficient predictive surrogate for fast impact-resistance evaluation of TPU composites and guidance of pre-production design towards impact. The following sub-sections will provide detailed explanations of each component.

3.1 Low-velocity impact tests

As illustrated in Figure 3, low-velocity impact tests were conducted in accordance with the ASTM D7136 standard using a drop-weight impact tower with a modified fixture setup.

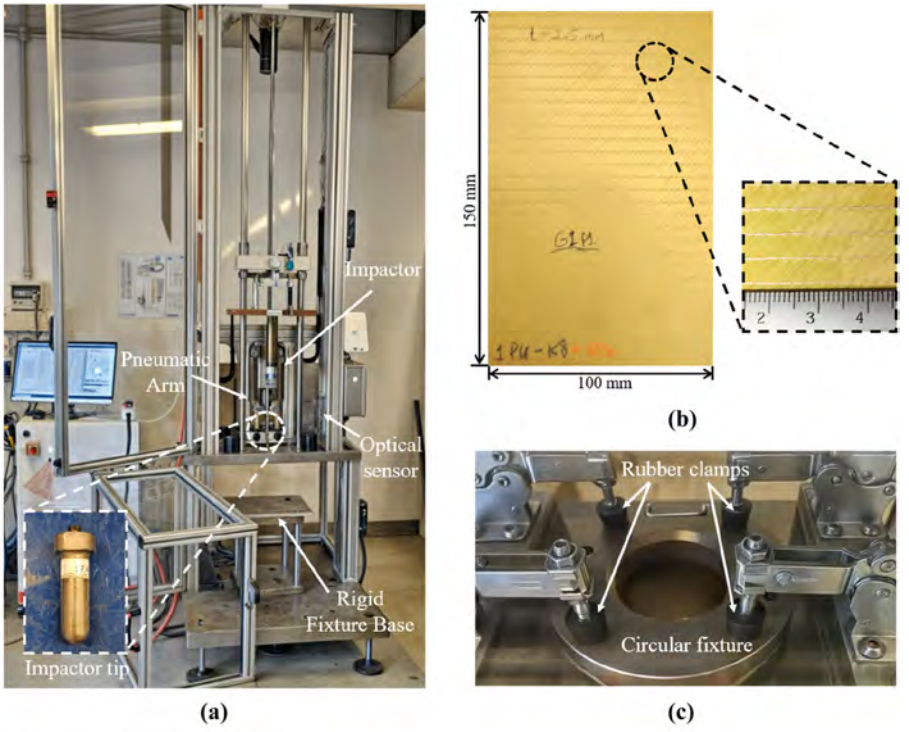

Source(s): Figure created by authors

Figure 3. (a) Drop-weight impact tower, (b) TPU composite specimen and (c) circular fixture

Downloaded from http://www.emerald.com/ijsi/article-pdf/doi/10.1108/IJSI-07-2025-0180/10416281/ijsi-07-2025-0180en.pdf by Politecnico di Milano user on 06 March 2026

Rectangular composite specimens (150 mm × 100 mm) were centrally impacted by a hemispherical impactor (diameter: 12.7 mm, weight: 5.47 kg). A sensor was used to measure the initial impact velocity upon contact with the laminate, while a load cell was employed to record the contact force between the impactor and the specimen. The tests were performed at three energy levels: 10 J, 20 J and 50 J. For each condition, three replicates were conducted to ensure repeatability and stability (Samlal and Santhanakrishnan, 2022; Meireman *et al*., 2024; Llanos *et al*., 2024). To prevent rebound-induced secondary impacts, a pneumatic arm was incorporated into the system. A circular fixture was employed to ensure stable positioning and firm fixation of the specimens during testing, as shown in Figure 3(c). This fixture featured a central opening with a diameter of 75 mm and was rigidly fastened in place using four rubber clamps that provided consistent clamping pressure to minimize specimen movement. Experimental outcomes, including impact velocity, displacement and absorbed energy, were derived and computed from the load cell and the sensor.

3.2 Numerical simulation

As shown in Figure 4, a three-dimensional FE model was constructed in LS-DYNA. Due to symmetry, only a quarter of the laminate geometry was constructed. In the simulation, the motion of the impactor was restricted to the translation along the vertical direction against the laminate's plane to eliminate any unintended in-plane displacement. For the composite laminate, a homogenized macroscopic ply-level model was developed, capturing the bi-layer cross-ply architecture of the studied aramid fabric and variations in TPU content.

Through measurements on the cross-sectional graphs of the laminates, 16 aramid plies were defined, each with a consistent thickness of 0.152 mm. Each pair of adjacent aramid plies represents a single layer of fabric in the laminate specimen, resulting in a total of 8 ply-couples. Within each couple, the fiber orientations were assigned to $+45°$ and $-45°$, corresponding to the fabric architecture. While the model integrates 7 TPU matrix plies, all laminate plies are modeled with 8-node solid bricks. Aramid plies use the constant-stress under-integrated formulation (ELFORM = 1). To mitigate shear and volumetric locking in the very thin TPU plies, the improved modified-strain solid is adopted (ELFORM = −2). Node merging was employed between adjacent plies to establish interface contact in laminates. As observed in

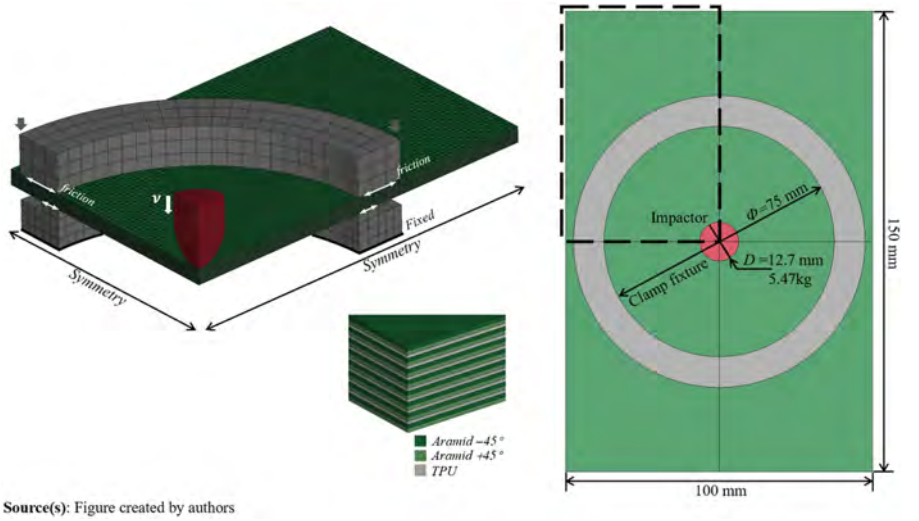

Source(s): Figure created by authors

Figure 4. Schematic of the quarter ply-level FE model for TPU composite LVI simulation

Downloaded from http://www.emerald.com/ijsi/article-pdf/doi/10.1108/IJSI-07-2025-0180/10416281/ijsi-07-2025-0180en.pdf by Politecnico di Milano user on 06 March 2026

Figure 1(b), the gaps between adjacent aramid layers are minimal in the K8_1PU case due to TPU material infiltration into the fabric during hot-press forming fabrication processing. In contrast, K8_2PU and K8_3PU both exhibit thick and measurable interlayer gap as the matrix content rises. Hence, to this evidence, these inter-ply TPU thicknesses were set as uniform values of 0.001 mm for K8_1PU and 0.060 mm and 0.104 mm for K8_2PU and K8_3PU, respectively. This FE model enables to tune the matrix content by altering TPU ply thicknesses, while the interlaminar failure can be described by the failure of these plies. To replicate the realistic experimental setup, the model also incorporated rigid circular clamps, as shown in Figure 4, and an automatic-surface-to-surface contact with a friction coefficient of 0.3 was defined at the contact interface (Kumar and Bijwe, 2011; Massaq *et al*., 2016). Hourglass modes can arise in FE models as a consequence of employing under-integrated element formulations. In this study, the Type 5 formulation with coefficient QH = 0.05 has been utilized: the Flanagan–Belytschko stiffness form with exact volume integration formulation. Mesh sensitivity analysis was conducted utilizing different-sized elements, in-depth explanation is not pursued herein. To balance reasonable accuracy and computational efficiency, a uniform mesh size of 1 mm × 1 mm × ply-thickness on composite laminate was adopted for the simulations.

For the material model, MAT 54/55(ENHANCED_COMPOSITE_DAMAGE) model is a recognized widely employed progressive damage material model in LS-DYNA for composite materials, which provides two failure theory options: Chang–Chang failure criteria (MAT 54) and Tsai–Wu failure criteria (MAT 55). In this study, MAT 55, which has been validated in many impact conditions (Sy *et al*., 2019; Berk *et al*., 2016), was adopted to describe the behavior of the studied aramid layer. Within the MAT 55 card, the modes of the tensile and compressive fiber are driven as in the Chang-Chang criteria (Chang and Chang, 1987), and the tensile and compressive matrix failures are defined by the Tsai–Wu criteria (Tsai and Wu, 1971). Damage evolution is governed through a set of residual stress limit factors (SLIMT1/2 = 0.1; SLIMC1/2 = 0.9; SLIMS = 0.6), which quantify the residual strength retained by the composite after meeting the failure criteria. As for the TPU inter-plies, MAT 3(PLASTIC_KINEMATIC) model was chosen, which is suitable for capturing the elastic–plastic response of isotropic materials (Hallquist, 2018). In the material model, the elastic and plastic behaviors are defined through Young's modulus and tangent modulus, respectively, while material failure is defined by the effective plastic strain. The input parameters for both the aramid and TPU were derived from standard characterization experiments. A summary of these properties is presented in Table 2.

After comparison and validation of the numerical simulations against experiment results, Livermore Software Optimization (LS-OPT) was employed to automate and streamline the impact simulation process in conjunction with LS-DYNA. LS-OPT is a standalone design-optimization and probabilistic-analysis software developed by Livermore Software Technology Corporation that interfaces directly with LS-DYNA to facilitate structured workflow, explore design spaces and manage simulation batches (Stander *et al*., 2020). In this study, LS-OPT was configured to iteratively launch explicit impact simulations across a predetermined range of energy levels, enabling efficient generation of a comprehensive dataset for training the neural networks. A detailed schematic of the LS-OPT workflow adopted in this study is provided in Figure 5. Deterministically and uniformly sampled impact energy levels, ranging from 10 J to 50 J at equal intervals (1.5 J), were employed as input variables (10 J, 20 J and 50 J levels were not included). A total of 78 virtual impact simulation cases, 26 for each laminate case, were conducted to construct the dataset used for subsequent ML.

3.3 Artificial neural network

In this study, ANN was utilized to predict the impact response of the TPU composites. The ANN employed was a feed-forward neural network developed in MATLAB. To train the

Downloaded from http://www.emerald.com/ijsi/article-pdf/doi/10.1108/IJSI-07-2025-0180/10416281/ijsi-07-2025-0180en.pdf by Politecnico di Milano user on 06 March 2026

Table 2. Material properties of aramid and TPU

Properties	Symbol	Unit	Value
DuPont Kevlar® XP S307 aramid composite laminate			
Density	ρ	kg/m^3	1,410
Young's modulus	E_a, E_b	*GPa*	21.83
Poisson's ratio	ν_{ba}		0.33
Shear modulus	G_{ab}	*MPa*	256.58
Longitudinal tensile strength	X_T	*MPa*	764.20
Longitudinal compressive strength	X_C	*MPa*	442.12
Transverse tensile strength	Y_T	*MPa*	764.20
Transverse compressive strength	Y_C	*MPa*	442.12
ManotoFlex TPU Grade 2198A			
Density	ρ	kg/m^3	1,230
Tensile modulus	E	*MPa*	120
Yield stress	σ_y	*MPa*	15
Ultimate tensile strength	σ_u	*MPa*	98
Elongation at Failure	*FS*	%	400

Source(s): Table created by authors

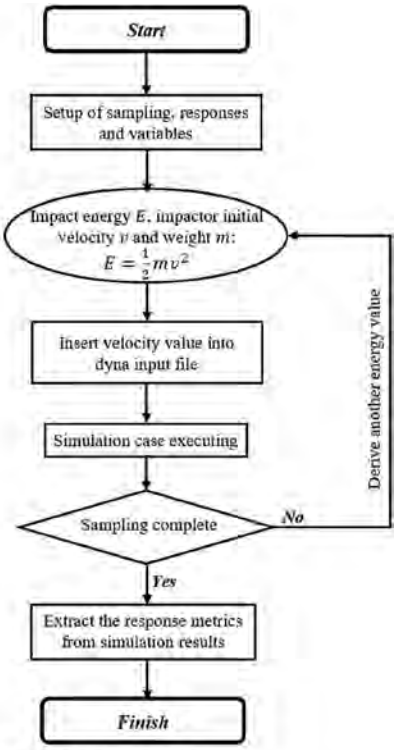

Source(s): Figure created by authors

Figure 5. LS-OPT work flowchart of automatic virtual LVI testing campaign and database generation for ANN

Downloaded from http://www.emerald.com/ijsi/article-pdf/doi/10.1108/IJSI-07-2025-0180/10416281/ijsi-07-2025-0180en.pdf by Politecnico di Milano user on 06 March 2026

network, two distinct optimization algorithms were implemented, compared and evaluated: Levenberg–Marquardt (LM) and SCG. These algorithms were selected due to their contrasting strengths: LM is renowned for its fast and accurate convergence, while SCG offers scalable optimization with lower memory demands. The loss function was defined by the mean squared error (MSE), as shown in Equation 1:

$$\mathrm{MSE} = \frac{1}{n}\sum_{i=1}^{n}(y_i - \widehat{y}_i)^2 \tag{1}$$

where y_j is the expected value, $\widehat{y_j}$ the output value predicted by the network and n the number of samples. For both algorithms, model performance was monitored and the weights were updated by minimizing the MSE.

3.3.1 Levenberg–Marquardt algorithm. The LM algorithm addresses non-linear least squares problems by integrating the Gauss–Newton method with gradient descent methods (Gavin, 2016). This hybrid approach enhances convergence stability and accuracy, rendering LM particularly effective for training neural networks requiring high precision. The gradient descent and Gauss–Newton update steps are formulated in Equations 2 and 3, respectively.

$$h_{\mathrm{GD}} = \alpha J^T \omega (y - \widehat{y}) \tag{2}$$

$$h_{\mathrm{GN}} = \left(J^T \omega J\right)^{-1} J^T \omega (y - \widehat{y}) \tag{3}$$

where J is the Jacobian matrix, ω is the weight, h is the perturbation. A damping parameter (λ) is introduced in Equation 4 to regulate the optimization process and ensure stable convergence. Both α in Equation 2 and λ in Equation 4 play similar roles within the algorithm. The selection of an appropriate λ is critical, and iterative schemes are typically employed to determine its optimal value. When λ is small, the algorithm behaves like Gauss–Newton, offering rapid convergence. When λ is large, it defaults to a more conservative gradient descent approach, ensuring stability near local minima. The LM algorithm exhibits a hybrid structure, which is characterized as follows:

$$\left(J^T \omega J + \lambda I\right) h_{\mathrm{LM}} = J^T \omega (y - \widehat{y}) \tag{4}$$

where h_{LM} is the perturbation of the LM. Similarly, in Equation (3), the second-order approximation of Equation (4) is defined by $J^T \omega J$. In cases involving multiple input variables, as employed in this study, it becomes necessary to update the Jacobian matrix J at each iteration. Utilizing Broyden's rank-1 update method, the Jacobian renewal can be formulated as follows:

$$J_n = J + \frac{[\widehat{y}(w+h) - \widehat{y}(w) - Jh]h^T}{h^T h} \tag{5}$$

where J_n is an updated Jacobian matrix of the first derivatives. This approximation avoids recomputing J from scratch at each iteration, reducing computational overhead without sacrificing significant accuracy. The distinguishing feature of the LM algorithm, in comparison to other optimization methods, is its capability to dynamically update the Jacobian matrix J during training. This adaptive mechanism enhances the algorithm's robustness by mitigating convergence difficulties commonly associated with fixed Jacobian approximations, thereby promoting stable and reliable performance across diverse datasets (Transtrum and Sethna, 2012).

3.3.2 Scaled conjugate gradient. The SCG algorithm is a member of the conjugate gradient family of optimization methods, designed to accelerate convergence without requiring

Downloaded from http://www.emerald.com/ijsi/article-pdf/doi/10.1108/IJSI-07-2025-0180/10416281/ijsi-07-2025-0180en.pdf by Politecnico di Milano user on 06 March 2026

expensive line searches at each iteration (Møller, 1993). This design lowers computational complexity, thereby improving efficiency. In the SCG algorithm, the step size is estimated using a quadratic approximation of the error criterion, which reduces reliance on user-defined parameters. These features render SCG a robust optimization method for neural network training, especially in scenarios where accelerated convergence is essential (Babani *et al.*, 2016).

The step size α_k in the SCG algorithm is specified in Equation 6, where $\overline{\omega}$ denotes the weight vector and $E(\overline{\omega})$ represents the global error function. The vectors $\overline{p_1}$, $\overline{p_2}$, $\overline{p_1}$,.. $\overline{p_k}$ are non-zero search directions and $\nabla E_{q\omega}(\overline{\omega})$ refers to the quadratic approximation of the error function. The parameters μ_k and δ_k govern the determination of the step size.

$$\alpha_k = \frac{\mu_k}{\delta_k} = \frac{-\overline{p_j}^T \nabla E_{q\omega}\left(\overline{\omega}\right)}{\overline{p_j}^T \nabla^2 E_{q\omega}\left(\overline{\omega}\right)\overline{p_j}} \tag{6}$$

The comparison parameter (Δ_k) serves as a measure of how closely the quadratic approximation aligns with the global error function $E(\overline{\omega}_k + \alpha_k \overline{p}_k)$.

$$\Delta_k = \frac{2\delta_k\left[E\left(\overline{\omega}_k\right) - E\left(\overline{\omega}_k + \alpha_k \overline{p}_k\right)\right]}{\mu_k^2} \tag{7}$$

If $\Delta_k \geq 0$, the step is accepted, and the algorithm proceeds. If $\Delta_k < 0$, the approximation is considered poor, and an alternative direction is chosen. This mechanism eliminates the need for repeated line searches while maintaining convergence efficiency (Oliver *et al.*, 2021).

4. Results and discussion

This section first characterizes the impact behaviors of TPU composites through combined experimental-numerical outcomes. Close agreement confirms the fidelity of the numerical approach and the ply-level FE model. The effect of matrix content on the laminate's impact resistance performance has then been explored and discussed. Subsequently, the FE-generated dataset is employed to train the neural network surrogate. By altering algorithms and network architecture, the performance and accuracy of the network has been evaluated to identify the optimal model. After all, the eventual network model has been tested against unseen experiment results, corroborating both the reliability of the proposed hybrid framework and the robustness of the surrogate model.

4.1 Experimental and numerical results

Table 3 compiles the comparison between the simulations and experiments on impact response feature values of peak force, peck displacement and energy absorption, and the comparison on detailed response histories across all impact scenarios is shown in Figure 6, including the force-time and force-displacement plots. From the plots in Figure 6, closed-shape force-displacement curves indicate that all the TPU composite specimens rebounded after impacts of up to 50 J without penetration, confirming the excellent dynamic impact-recovery behavior. Compared with studies on Kevlar-fiber composite with the thermoset matrix, severe fiber breakage and perforation started from 37 J impact on even thicker laminate (Rezasefat *et al.*, 2022b), underscoring the TPU toughening properties on composite impact enhancement and effectiveness in delaying damage initiation. Both the statistics and the curves reveal that increasing the impact energy raises the peak impact force and deflection. While the ascending portions of the force–displacement traces nearly coincide across the energy levels, demonstrating the stability and continuity of the laminate's impact stiffness, together with

Downloaded from http://www.emerald.com/ijsi/article-pdf/doi/10.1108/IJSI-07-2025-0180/10416281/ijsi-07-2025-0180en.pdf by Politecnico di Milano user on 06 March 2026

Table 3. Experimental and numerical comparison on key impact response parameters with deviation

	Impact energy	Peak force [N] K8_1PU		K8_2PU		K8_3PU	
Experiment	10 J	2346.12	6.96%	2607.82	1.92%	2859.22	4.62%
Simulation		2183.85		2557.96		2727.84	
Experiment	20 J	3571.24	1.40%	3888.32	3.98%	4067.94	1.38%
Simulation		3521.86		3733.84		4124.53	
Experiment	50 J	5669.45	9.64%	6445.48	9.88%	7011.71	5.83%
Simulation		5122.74		5797.92		6602.82	

	Impact Energy	Peak displacement [mm] K8_1PU		K8_2PU		K8_3PU	
Experiment	10 J	10.06	1.19%	9.51	4.62%	8.52	0.58%
Simulation		9.94		9.07		8.47	
Experiment	20 J	13.31	1.12%	13.07	0.68%	11.02	0.99%
Simulation		13.16		12.98		11.13	
Experiment	50 J	20.95	3.44%	19.47	0.67%	17.12	3.71%
Simulation		20.23		19.34		17.78	

	Impact Energy	Absorbed energy [J] K8_1PU		K8_2PU		K8_3PU	
Experiment	10 J	4.35	5.07%	3.95	5.18%	3.46	5.08%
Simulation		4.86		3.43		2.95	
Experiment	20 J	12.70	4.85%	11.96	4.91%	11.16	1.50%
Simulation		13.67		10.98		10.86	
Experiment	50 J	42.15	4.99%	40.35	2.11%	38.05	4.41%
Simulation		44.71		39.27		35.79	

Source(s): Table created by authors

the evidence that the force–time and force–displacement records are remarkably smooth, exhibiting neither oscillations nor abrupt drops indicative of catastrophic internal failure. Post-impact inspections corroborate the absence of fiber breakage or delamination, suggesting the composite's superior impact resistance performance attributing to the TPU material.

As shown in Figure 6, the simulated curves generally exhibit close agreement with the experimental results regarding overall shape, trends and key feature points, thus validating the reliability of the ply-level modeling approach and the FE model. However, it should also be noted that under the high-energy 50 J impact scenario, a noticeable discrepancy emerges at the peak force. Specifically, the experimental force-displacement curves exhibit a pronounced sharp peak at the maximum force, whereas the simulation curves display a smoother transition, consequently underestimating the peak force. Such a discrepancy is not observed in lower-energy impact cases. Experimental observations suggest that during impact loading, the laminate undergoes sliding relative to the clamp fixture, moving towards the center during loading and backward during the rebound phase. This sliding behavior is particularly pronounced in high-energy impact cases. Despite rigorous attempts to secure and tighten the rubber clamps throughout the tests, this sliding could not be entirely eliminated, thereby introducing a limitation on the simulation's ability to precisely replicate significant sliding phenomena.

In Table 3, it also reveals that at the same impact energy level, laminates with higher TPU matrix content exhibit increased peak force, reduced displacement and absorbed energy, suggesting an increase in the rebounding-released energy. Leveraging the elastic properties of

Downloaded from http://www.emerald.com/ijsi/article-pdf/doi/10.1108/IJSI-07-2025-0180/10416281/ijsi-07-2025-0180en.pdf by Politecnico di Milano user on 06 March 2026

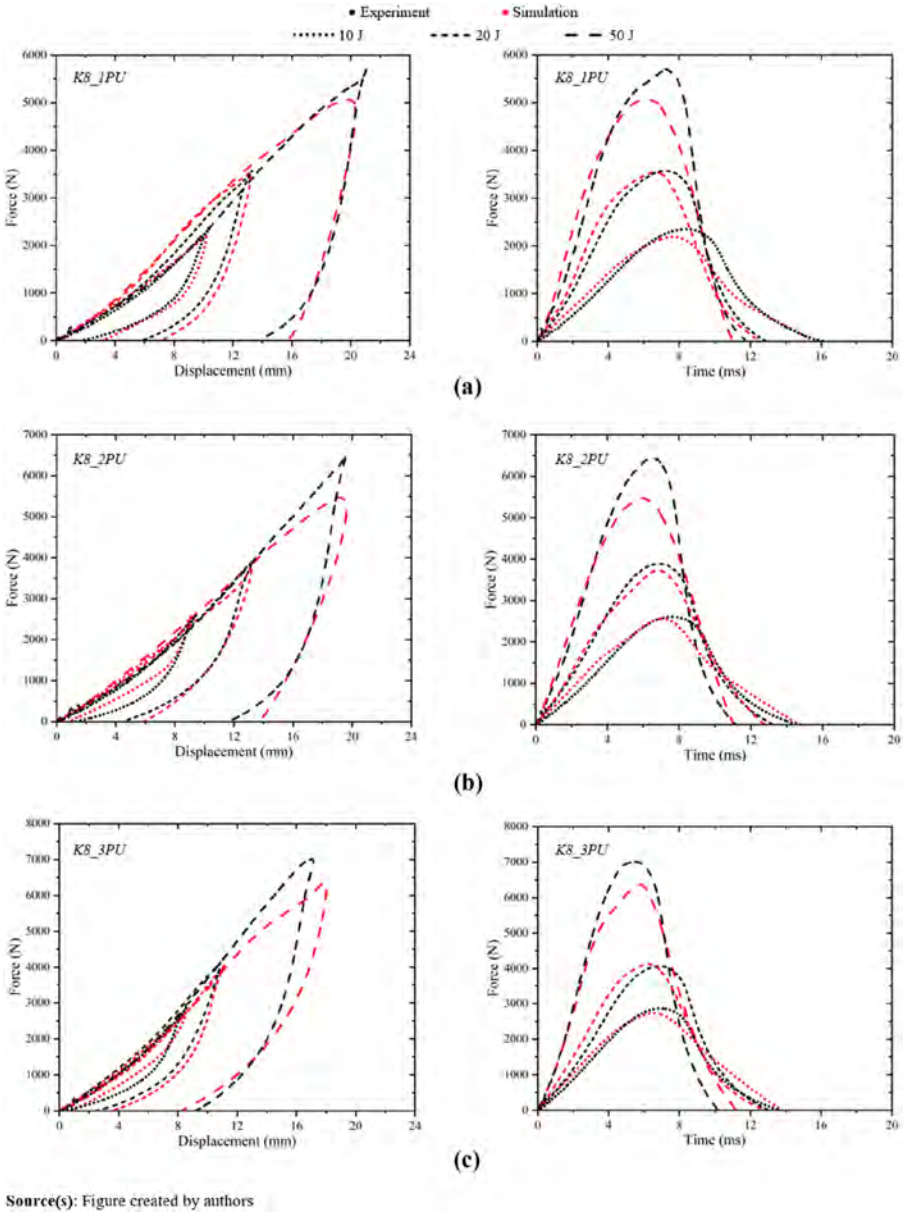

Source(s): Figure created by authors

Figure 6. Comparison of numerical and experimental results at 10 J, 20 J and 50 J: (a) K8_1PU, (b) K8_2PU and (c) K8_3PU

TPU, a greater matrix content enables the matrix to sustain a larger proportion of the impact load. During the rebound phase, the accumulated energy is elastically released, thereby decreasing the impact energy transmitted to the aramid fibers. Consequently, higher matrix content effectively reduces final residual deformation and the proportion of energy absorbed. Impact tolerance of composites, characterized by peak force and displacement, is an essential

Downloaded from http://www.emerald.com/ijsi/article-pdf/doi/10.1108/IJSI-07-2025-0180/10416281/ijsi-07-2025-0180en.pdf by Politecnico di Milano user on 06 March 2026

indicator of impact resistance performance. To further elucidate the role of TPU matrix content, Figure 7 presents a line-symbol plot of the impact tolerance point in three configurations across various impact scenarios. It is clearly observed that laminates with increasing TPU matrix content exhibit higher peak forces and less maximum displacement. This trend indicates the enhanced impact stiffness of the laminate, highlighting the robust influence of TPU on the evolution of the laminate's impact tolerance.

This subsection investigates the impact behavior of TPU composites, emphasizing the influence of the TPU matrix, while concurrently validating the reliability of the proposed ply-level numerical model. Drawing on considerations of impact-resistant performance evaluation, three key response metrics, peak impact force, maximum displacement and energy absorption ratio, were identified to characterize the mechanical response of the laminates under impacts. These metrics subsequently define the response space for the further neural network learning.

4.2 Neural network surrogate modeling and prediction performance

Following validation of the FE modeling approach, the developed model was employed in a virtual testing campaign using LS-OPT to generate the dataset for neural network surrogate model training. The neural network inputs include impact energy and the TPU matrix volume fraction. Three critical response metrics derived from simulation outcomes constitute the prediction space of the network, as shown in Figure 8. After the trail-and-error procedure on identifying the initial architecture of networks, a one-hidden-layer fully-connected network was selected as the initial architecture, as depicted in Figure 9. The total data of 78 observations were partitioned into 3 subsets: 69% (54 samples) for training, 21% (16 samples) for validation and the remaining 10% (8 samples) for testing. Prior to network training, normalization of both input and output parameters was essential, which ensures stable network performance, facilitates efficient convergence and maintains the relative relationships among features, thus promoting the reliability and generalizability of the training results. Accordingly, min-max normalization was applied in this study to rescale each feature to the range [0, 1], according to Equation 8:

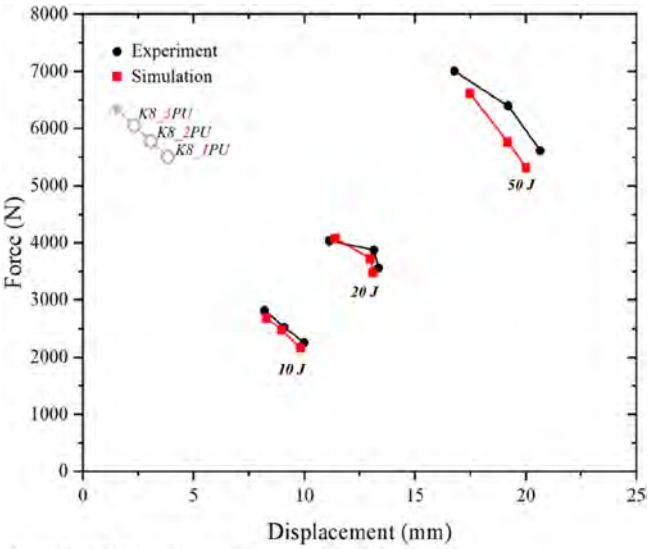

Source(s): Figure created by authors

Figure 7. The impact tolerance of TPU composites across different energy impacts

Downloaded from http://www.emerald.com/ijsi/article-pdf/doi/10.1108/IJSI-07-2025-0180/10416281/ijsi-07-2025-0180en.pdf by Politecnico di Milano user on 06 March 2026

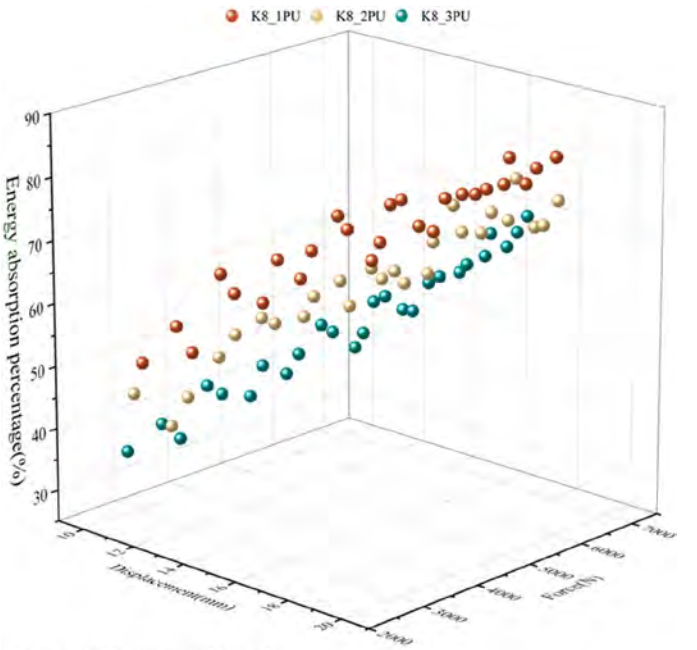

Source(s): Figure created by authors

Figure 8. The prediction response space for neural network learning

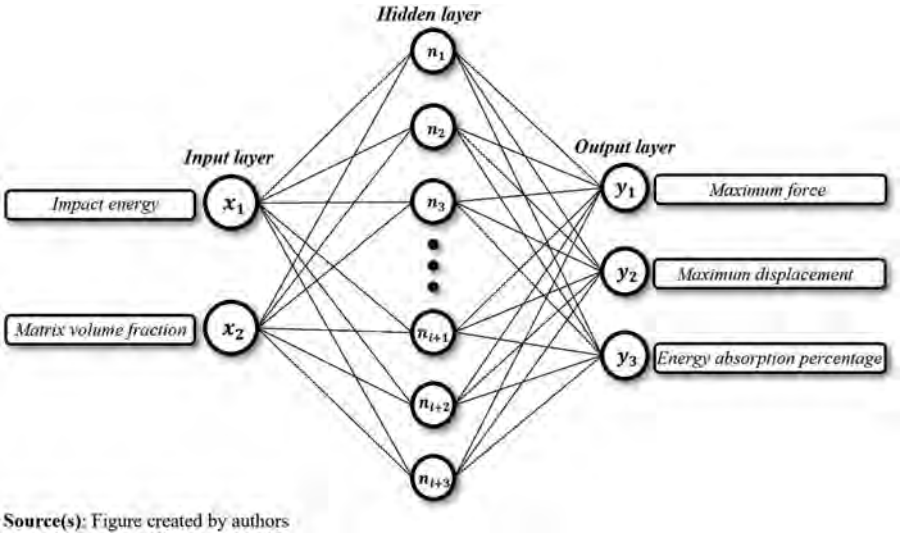

Source(s): Figure created by authors

Figure 9. The utilized neural network architecture

Downloaded from http://www.emerald.com/ijsi/article-pdf/doi/10.1108/IJSI-07-2025-0180/10416281/ijsi-07-2025-0180en.pdf by Politecnico di Milano user on 06 March 2026

$$x' = \frac{x_i - x_{min}}{x_{max} - x_{min}} \tag{8}$$

where x_i represents the original value, x' is the normalized value and x_{min} and x_{max} are the minimum and maximum values within the training set.

The size of the hidden layer, characterized by the number of hidden-layer neurons, significantly influences the predictive performance of a neural network model. Determining the optimal number of neurons, however, remains challenging and typically relies on the developer's expertise and trial, as currently there is no definitive theoretical guidance for calculating the accurate size for best performance. An insufficient number of neurons may prevent the neural network from adequately identifying meaningful patterns within complex datasets, resulting in underfitting. Conversely, an excessively large number of neurons can lead to overfitting, wherein the network's extensive processing capacity exceeds the informational content available within the training dataset. In this study, varying numbers of hidden-layer neurons were employed, trained and tested using LM and SCG algorithms. The network performance evaluated through MSE for training and validation subsets is presented in Figure 10. Results indicate that network performance initially improves with increasing hidden-layer size for both algorithms. Specifically, the LM algorithm achieves its lowest validation MSE of 0.0029 with 10 neurons, whereas the SCG algorithm attains its minimum MSE of around 0.0031 with 12 neurons. These values correspond to the optimal network capacities for each respective algorithm. Increasing the hidden-layer size beyond these points did not yield further improvement; instead, the MSE began to increase, signifying the onset of overfitting.

Figure 11 shows MSE curves over epoch for each algorithm with optimal architecture. Training was terminated based on an early-stopping criterion that monitored validation error, and the network state corresponding to the lowest validation MSE was retained as the best model. For the LM algorithm, the best validation performance was achieved at epoch 27, whereas for the SCG algorithm, the optimal validation performance occurred at epoch 38. The quality of the prediction was further evaluated through regression plots, as illustrated in

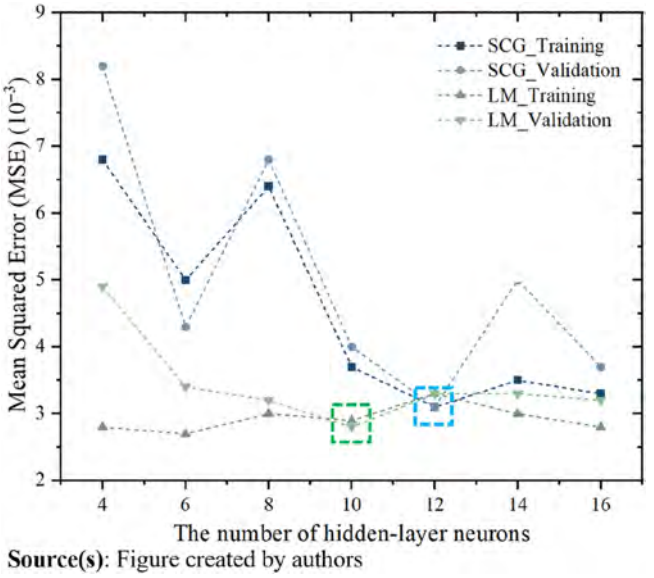

Source(s): Figure created by authors

Figure 10. Comparison on MSE of networks with LM and SCG algorithms under different hidden-layer size

Downloaded from http://www.emerald.com/ijsi/article-pdf/doi/10.1108/IJSI-07-2025-0180/10416281/ijsi-07-2025-0180en.pdf by Politecnico di Milano user on 06 March 2026

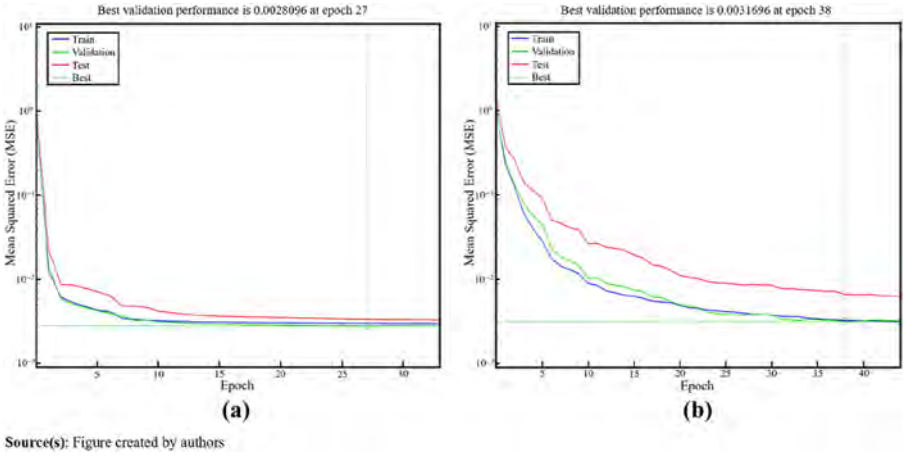

Figure 11. MSE curves over epoch: (a) LM network with 10-neuron hidden layer and (b) SCG network with 12-neuron hidden layer

Figure 12. The neural network trained using LM algorithm demonstrated an exceptional fit, with data points aligning closely to the bisector line in the prediction-expectation plots and achieving consistently high correlation coefficients of approximately 0.986. This suggests that the LM network predictions exhibit nearly perfect correlation with the target responses. Conversely, the SCG network showed a somewhat reduced correlation with target responses, with correlation coefficients ranging from 0.97 to 0.93. Although still respectable, this lower

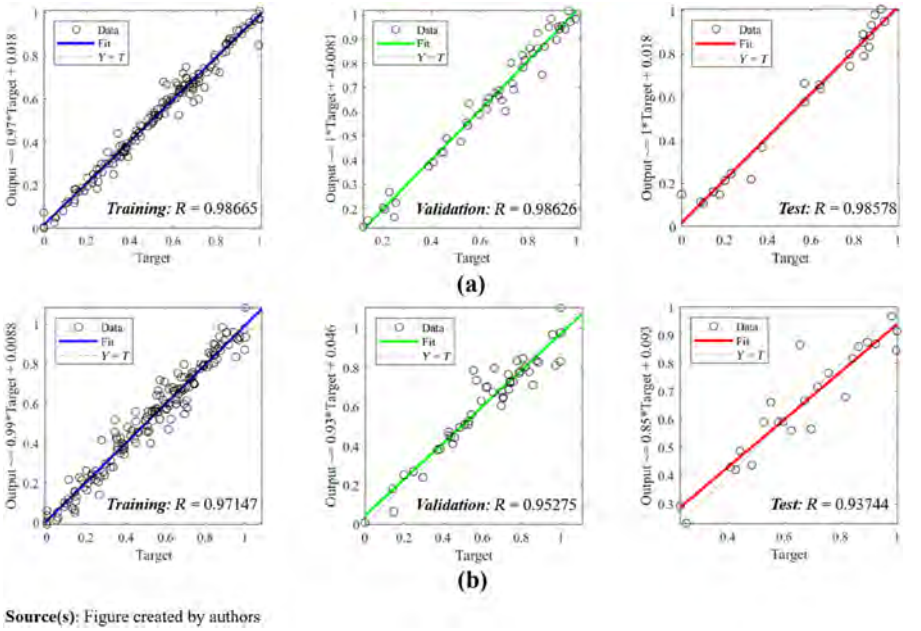

Figure 12. Regression plots: Comparison of the target and prediction: (a) LM network model and (b) SCG network model

Downloaded from http://www.emerald.com/ijsi/article-pdf/doi/10.1108/IJSI-07-2025-0180/10416281/ijsi-07-2025-0180en.pdf by Politecnico di Milano user on 06 March 2026

correlation was accompanied by increased scatter in the regression plots, particularly evident within the test dataset, indicating greater deviations between the predicted and actual target values.

Based on the preceding analysis, the trained LM network with a 10-neuron hidden layer is identified to be the best-performing predictive surrogate model. At last, as shown in Figure 13, this FE-guided surrogate prediction results have been compared against unseen experimental results regarding the impact response metrices. The model's predictions nicely aligned with the experimental observations, yielding a correlation coefficient of 0.96. This strong agreement underscores the robustness and accuracy of the proposed surrogate model in capturing and predicting the impact responses of TPU composites with varying matrix content.

5. Conclusion

This study proposes and validates a comprehensive hybrid framework that combines experimental testing, FE modeling and ANNs to investigate and effectively predict the low-velocity impact responses of Kevlar fiber thermoplastic composites incorporating varying TPU matrix content. Key findings include:

(1) According to the mechanical behaviors under impacts, the TPU composites exhibit exceptional toughening and superior impact resistance, while increasing TPU matrix content can effectively enhance composite impact stiffness and modulate impact tolerance.

(2) The developed macro-homogeneous ply-level FE model can accurately capture and replicate the impact behavior and response of TPU composites, serving as a high-fidelity virtual testing tool to simulate impact cases with physical accuracy.

(3) The FE-guided neural network using the LM algorithm demonstrates excellent predictive accuracy and rapid convergence, facilitating a robust and efficient

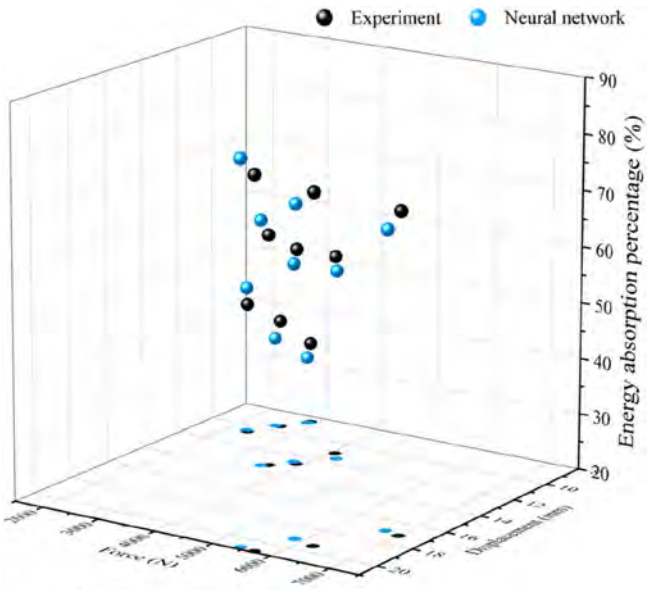

Source(s): Figure created by authors

Figure 13. Comparison on FE-guided LM neural network prediction against experimental results

Downloaded from http://www.emerald.com/ijsi/article-pdf/doi/10.1108/IJSI-07-2025-0180/10416281/ijsi-07-2025-0180en.pdf by Politecnico di Milano user on 06 March 2026

predictive surrogate model for composite instant impact resistance evaluation and design guidance.

This study also presents a robust strategy for exploring, investigating, and predicting the impact performance of advanced composite materials. The numerical results from validated numerical models with detailed experimental data can be utilized as a dataset for ML, thereby enabling rapid prediction of complex impact behaviors.

References

Al-Dhaheri, M.A., Cantwell, W.J., Barsoum, I. and Umer, R. (2024), "Characterization of relaxation behaviour of CF/PEKK aerospace composites using the time-temperature-crystallinity superposition principle", *Journal of Composite Materials*, Vol. 58 No. 18, pp. 2061-2077, doi: 10.1177/00219983241260555.

Ali, R., Iannace, S. and Nicolais, L. (2003), "Effects of processing conditions on the impregnation of glass fibre mat in extrusion/calendering and film stacking operations", *Composites Science and Technology*, Vol. 63 No. 15, pp. 2217-2222, doi: 10.1016/s0266-3538(03)00175-1.

Babani, L., Jadhav, S. and Chaudhari, B. (2016), "Scaled conjugate gradient based adaptive ANN control for SVM-DTC induction motor drive", *Neurocomputing*, Vol. 112, pp. 384-395, doi: 10.1007/978-3-319-44944-9_33.

Berk, B., Karakuzu, R., Murat Icten, B., Arikan, V., Arman, Y., Atas, C. and Goren, A. (2016), "An experimental and numerical investigation on low velocity impact behavior of composite plates", *Journal of Composite Materials*, Vol. 50 No. 25, pp. 3551-3559, doi: 10.1177/0021998315622805.

Boria, S., Obradovic, J. and Belingardi, G. (2015), "Experimental and numerical investigations of the impact behaviour of composite frontal crash structures", *Composites, Part B: Engineering*, Vol. 79, pp. 20-27, doi: 10.1016/j.compositesb.2015.04.016.

Boria, S., Scattina, A. and Belingardi, G. (2017), "Impact behavior of a fully thermoplastic composite", *Composite Structures*, Vol. 167, pp. 63-75, doi: 10.1016/j.compstruct.2017.01.083.

Boukar, A., Corn, S., Slangen, P.R. and Ienny, P. (2022), "Finite element modelling of low-velocity impact test on biaxial glass fiber-reinforced laminates", *International Journal of Impact Engineering*, Vol. 165, 104218, doi: 10.1016/j.ijimpeng.2022.104218.

Chang, F.-k. and Chang, K.-Y. (1987), "Laminated composites containing stress concentrations", *Journal of Composite Materials*, Vol. 21 September, pp. 834-855, doi: 10.1177/002199838702100904.

Ding, X., Hou, X., Xia, M., Ismail, Y. and Ye, J. (2022), "Predictions of macroscopic mechanical properties and microscopic cracks of unidirectional fibre-reinforced polymer composites using deep neural network (DNN)", *Composite Structures*, Vol. 302, 116248, doi: 10.1016/j.compstruct.2022.116248.

Gavin, H.P. (2016), *The Levenberg-Marquardt Method for Nonlinear Least Squares Curve-Fitting Problems*, Department of Civil and Environmental Engineering, Duke University.

Goodman, K.E. and Loos, A.C. (1990), "Thermoplastic prepreg manufacture", *Journal of Thermoplastic Composite Materials*, Vol. 3 No. 1, pp. 34-40, doi: 10.1177/089270579000300104.

Hallquist, J.O. (2018), "Livermore software Technology corporation (LSTC)", *LS-DYNA Keyword User's Manual Volume I&II*, Vols I&IIOctober, pp. 1-1619.

Han, L., Qi, H., Yang, J., Chu, F., Lin, C., Liu, P. and Zhang, Q. (2024), "Study on the low-velocity impact response and damage mechanisms of thermoplastic composites", *Polymer*, Vol. 16 No. 6, 791, doi: 10.3390/polym16060791.

Hasebe, S., Higuchi, R., Yokozeki, T. and Takeda, S. (2025), "Prediction of compression after impact strength from surface profile of low-velocity impact damaged CFRP laminates using machine learning", *Composer Part A*, Vol. 189, 108560, doi: 10.1016/j.compositesa.2024.108560.

Downloaded from http://www.emerald.com/ijsi/article-pdf/doi/10.1108/IJSI-07-2025-0180/10416281/ijsi-07-2025-0180en.pdf by Politecnico di Milano user on 06 March 2026

Hazzard, M.K., Hallett, S., Curtis, P.T., Iannucci, L. and Trask, R.S. (2017), "Effect of fibre orientation on the low velocity impact response of thin Dyneema® composite laminates", *International Journal of Impact Engineering*, Vol. 100, pp. 35-45, doi: 10.1016/j.ijimpeng.2016.10.007.

Karsandik, Y., Sabuncuoglu, B., Yildirim, B. and Silberschmidt, V.V. (2023), "Impact behavior of sandwich composites for aviation applications: a review", *Composite Structures*, Vol. 314, 116941, doi: 10.1016/j.compstruct.2023.116941.

Kumar, M. and Bijwe, J. (2011), "Composite friction materials based on metallic fillers: sensitivity of μ to operating variables", *Tribology International*, Vol. 44 No. 2, pp. 106-113, doi: 10.1016/j.triboint.2010.09.013.

Kumar, Y., Rezasefat, M., Amico, S.C., Manes, A., Dolez, P.I. and Hogan, J.D. (2024), "Comparison of two progressive damage models for predicting low-velocity impact behavior of woven composites", *Thin-Walled Structures*, Vol. 197, 111611, doi: 10.1016/j.tws.2024.111611.

Kurdiş, M.M., Ulus, H. and Avcı, A. (2025), "Development of innovative thermoplastic Elium® nanocomposites reinforced with Ag/SiC-doped PAN nanofibers: advancing mechanical properties and X-ray shielding performance", *Fibers and Polymers*, Vol. 26 No. 6, pp. 2581-2594, doi: 10.1007/s12221-025-00972-7.

Lei, X.D., Wu, X.Q., Zhang, Z., Xiao, K.L., Wang, Y.W. and Huang, C.G. (2021), "A machine learning model for predicting the ballistic impact resistance of unidirectional fiber-reinforced composite plate", *Scientific Reports*, Vol. 11 No. 1, p. 6503, doi: 10.1038/s41598-021-85963-3.

Lin, Y.Y., Lin, M.-C., Lou, C.-W., Chen, Y.S. and Lin, J.H. (2023), "Thermoplastic laminated composites applied to impact resistant protective gear: structural design and development", *Polymers*, Vol. 15 No. 2, p. 292, doi: 10.3390/polym15020292.

Liu, L., Hu, D., Wan, D., Hu, X. and Han, X. (2021), "Low velocity impact behavior and simulation of parametric effect analysis for UHMWPE/LLDPE thermoplastic composite laminates", *Composite Structures*, Vol. 258, 113180, doi: 10.1016/j.compstruct.2020.113180.

Llanos, J.J., Wang, K. and Taheri, F. (2024), "Characterization of low- and high-velocity responses of basalt–epoxy and basalt–elium composites", *Polymers*, Vol. 16 No. 7, p. 926, doi: 10.3390/polym16070926.

Lu, T., Xue, L., Ning, H., Wu, X., Ding, Z., Hu, N., Zhao, L. and Qi, X. (2025), "Optimizing thickness and interlayer placement of electrospun TPU nanofibrous membranes for enhanced interlaminar performance and impact resistance in CFRP laminates", *Polymer Composites*, pp. 1-16, e70172, doi: 10.1002/pc.70172.

Massaq, A., Rusinek, A., Klosak, M., Abed, F. and El Mansori, M. (2016), "A study of friction between composite-steel surfaces at high impact velocities", *Tribology International*, Vol. 102, pp. 38-43, doi: 10.1016/j.triboint.2016.05.011.

Meireman, T., Verboven, E., Kersemans, M., Van Paepegem, W., De Clerck, K. and Daelemans, L. (2024), "Low-velocity impact resistance and compression after impact strength of thermoplastic nanofiber toughened carbon/epoxy composites with different layups", *Polymers*, Vol. 16 No. 21, 3060, doi: 10.3390/polym16213060.

Mezeix, L., Soldevila, A.S., Relandeau, A. and Bouvet, C. (2023), "A new method to predict damage to composite structures using convolutional neural networks", *Materials*, Vol. 16 No. 1, p. 45.

Miller, S.G., Roberts, G.D., Kohlman, L.W., Heimann, P.J., Pereira, J.M., Ruggeri, C.R., Martin, R.E. and McCorkle, L.S. (2015), "Impact behavior of composite fan blade leading edge subcomponent with thermoplastic polyurethane interleave", *Proceedings of ICCM20-20th International Conference on Composite Materials*, Copenhagen.

Møller, M.F. (1993), "A scaled conjugate gradient algorithm for fast supervised learning", *Neural Networks*, Vol. 6 No. 4, pp. 525-533, doi: 10.1016/s0893-6080(05)80056-5.

Montazeri, A., Ahmadian, I., Bahmanpour, E., Saeedi, A. and Safarabadi, M. (2025a), "Mechanical behaviors of star honeycombs with symmetry-broken lattices", *European Journal of Mechanics - A: Solids*, Vol. 113, 105709, doi: 10.1016/j.euromechsol.2025.105709.

Downloaded from http://www.emerald.com/ijsi/article-pdf/doi/10.1108/IJSI-07-2025-0180/10416281/ijsi-07-2025-0180en.pdf by Politecnico di Milano user on 06 March 2026

Montazeri, A., Rahimi, M., Maghzi, M., Ahmadian, I. and Safarabadi, M. (2025b), "Aperiodic ordered lattices with semi Re-entrant einstein monotile", *European Journal of Mechanics - A: Solids*, Vol. 115, 105830, doi: 10.1016/j.euromechsol.2025.105830.

Oliver, G.A., Ancelotti, A.C., Jr and Gomes, G.F. (2021), "Neural network-based damage identification in composite laminated plates using frequency shifts", *Neural Computing and Applications*, Vol. 33 No. 8, pp. 3183-3194, doi: 10.1007/s00521-020-05180-3.

Paolo, F., Wade, B., Deleo, F., Rassaian, M., Higgins, M. and Byar, A. (2011), "LS-DYNA MAT54 modeling of the axial crushing of a composite tape sinusoidal specimen", *Composites Part A: Applied Science and Manufacturing*, Vol. 42 No. 11, pp. 1809-1825, doi: 10.1016/j.compositesa.2011.08.004.

Pechlivani, E.M. (2024), "3D printing TPU composites with continuous carbon fibers for impact absorption applications", *Int. J. Mod. Manuf. Technol.*, Vol. 16 No. 3, pp. 40-46, doi: 10.54684/ijmmt.2024.16.3.40.

Pittie, T., Kartikeya, K., Bhatnagar, N., Krishnan, N.A., Senthil, T. and Rajan, S.D. (2023), "Building a predictive soft armor finite element model combining experiments, simulations, and machine learning", *Journal of Composite Materials*, Vol. 57 No. 9, pp. 1599-1615, doi: 10.1177/00219983231160497.

Qiu, C., Han, Y., Shanmugam, L., Zhao, Y., Dong, S., Du, S. and Yang, J. (2022), "A deep learning-based composite design strategy for efficient selection of material and layup sequences from a given database", *Composites Science and Technology*, Vol. 226, 109154, doi: 10.1016/j.compscitech.2021.109154.

Rezasefat, M., Jimenez, A.G. and Ma, D. (2022a), "Experimental study on the low-velocity impact response of inter-ply S2-glass/aramid woven fabric hybrid laminates", *Thin Struct*, Vol. 177, 109458.

Rezasefat, M., Jimenez, A.G., Ma, D., Vescovini, A., Lomazzi, L., da Silva, A.A., Amico, S.C. and Manes, A. (2022b), Experimental study on the low-velocity impact response of inter-ply S2-glass/aramid woven fabric hybrid laminates, *Thin-Walled Structures*, Vol. 177, 109458, doi: 10.1016/j.tws.2022.109458.

Rizzo, F., Agostino, T.D., Cuomo, S., Pinto, F. and Meo, M. (2020), "High-velocity impact investigation on thermoplastic polyurethane/CFRP T-stiffened panel", *Materials Today: Proceedings*, pp. 2214-7853.

Russo, P., Langella, A., Papa, I., Simeoli, G. and Lopresto, V. (2016), "Low-velocity impact and flexural properties of thermoplastic polyurethane/woven glass fabric composite laminates", *Procedia Engineering*, Vol. 167, pp. 190-196, doi: 10.1016/j.proeng.2016.11.687.

Samlal, S. and Santhanakrishnan, R. (2022), "Low-velocity impact behavior of foam core sandwich panels with inter-ply and intra-ply carbon/kevlar/epoxy hybrid face sheets", *Polymers*, Vol. 14 No. 5, 1060, doi: 10.3390/polym14051060.

Senol, H., Ulus, H., Yildirim, C., Al-Nadhari, A., Topal, S. and Yildiz, M. (2025a), "Assessing fracture toughness performance of adhesively bonded carbon fiber/epoxy composite joints accompanied by acoustic emission inspection: effect of surface treatment methods", *Engineering Fracture Mechanics*, Vol. 321, 111119, doi: 10.1016/j.engfracmech.2025.111119.

Senol, H., Ulus, H., Al-Nadhari, A., Topal, S. and Yildiz, M. (2025b), "Ameliorating tensile and fracture performance of carbon fiber–epoxy composites via atmospheric plasma activation: insights into damage modes through in-situ acoustic emission inspection", *Composer Part A*, Vol. 195, 108929, doi: 10.1016/j.compositesa.2025.108929.

Şenyurt, M.A., Kurdiş, M.M., Ulus, H. and Avcı, A. (2025), "Enhanced mechanical and shape memory properties of Elium® nanocomposites reinforced with graphene and iron (II, III) oxide-doped polyacrylonitrile nanofibers", *Fibers and Polymers*, Vol. 26 No. 5, pp. 2097-2116, doi: 10.1007/s12221-025-00926-z.

Shah, S., Megat-Yusoff, P., Karuppanan, S., Choudhry, R., Ahmad, F., Sajid, Z., Gerard, P. and Sharp, K. (2021), "Performance comparison of resin-infused thermoplastic and thermoset 3D fabric composites under impact loading", *International Journal of Mechanical Sciences*, Vol. 189, 105984, doi: 10.1016/j.ijmecsci.2020.105984.

Downloaded from http://www.emerald.com/ijsi/article-pdf/doi/10.1108/IJSI-07-2025-0180/10416281/ijsi-07-2025-0180en.pdf by Politecnico di Milano user on 06 March 2026

Siengchin, S. (2023), "A review on lightweight materials for defence applications: a present and future developments", *Defence Technology*, Vol. 24, pp. 1-17, doi: 10.1016/j.dt.2023.02.025.

Sorour, S.S., Saleh, C.A. and Shazly, M. (2024), "A review on machine learning implementation for predicting and optimizing the mechanical behaviour of laminated fiber-reinforced polymer composites", *Heliyon*, Vol. 10 No. 13, e33681, doi: 10.1016/j.heliyon.2024.e33681.

Stander, N., Roux, W. and Basudhar, A. (2020), *LS-OPT User's Manual, Version 7.0*, Livermore Software Technology Corporation, Livermore, CA.

Staroverov, O., Lobanov, D., Strungar, E. and Lunegova, E. (2022), "Evaluation of the influence of preliminary low-velocity impacts on the residual fatigue life of CFRP composites", *Int. J. Struct. Integrity*, Vol. 14 No. 1, pp. 44-56, doi: 10.1108/ijsi-04-2022-0056.

Stephen, C., Thekkuden, D.T., Mourad, A.-H.I., Shivamurthy, B., Selvam, R. and Behara, S.R. (2022), "Prediction of impact performance of fiber reinforced polymer composites using finite element analysis and artificial neural network", *Journal of the Brazilian Society of Mechanical Sciences and Engineering*, Vol. 44 No. 9, p. 408, doi: 10.1007/s40430-022-03711-8.

Sun, X.C., Kawashita, L.F., Kaddour, A.S., Hiley, M.J. and Hallett, S.R. (2018), "Comparison of low velocity impact modelling techniques for thermoplastic and thermoset polymer composites", *Composite Structures*, Vol. 203, pp. 659-671, doi: 10.1016/j.compstruct.2018.07.054.

Sy, B.L., Fawaz, Z. and Bougherara, H. (2019), "Numerical simulation correlating the low velocity impact behaviour of flax/epoxy laminates", *Composites*, Vol. A 126, 105582, doi: 10.1016/j.compositesa.2019.105582.

Texier, A., Davis, R.M., Lyon, K.R., Gungor, A., McGrath, J.E., Marand, H. and Riffle, J.S. (1993), "Fabrication of PEEK/carbon fibre composites by aqueous suspension prepregging", *Polymer*, Vol. 34 No. 4, pp. 896-906, doi: 10.1016/0032-3861(93)90378-n.

Transtrum, M.K. and Sethna, J.P. (2012), "Improvements to the Levenberg-Marquardt algorithm for nonlinear least-squares minimization", *Journal of Computational Physics*, Vol. 231, pp. 297-312.

Tsai, S.W. and Wu, E.M. (1971), "A general theory of strength for anisotropic materials", *Journal of Composite Materials*, Vol. 5 No. 1, pp. 58-80, doi: 10.1177/002199837100500106.

Xiong, Y., Yang, H., Li, X., Lei, H. and Lu, G. (2023), "Crashworthy optimization of skeleton-filled FRP tubes based on back propagation neural network", *Heliyon*, Vol. 9 No. 12, e23019, doi: 10.1016/j.heliyon.2023.e23019.

Yakin, F.E., Senol, C.O., Birgun, N., Ulus, H., Yildiz, M. and Sas Cayci, H.S. (2025), "Influence of stacking sequence and compaction force during the AFP process on mechanical performance and damage mechanisms elucidated by acoustic emission insights", *Proc. IMechE Part L: J. Mater. Des. Appl.*, doi: 10.1177/14644207241309548.

Yildirim, C., Sas, H.S., Şenyurt, M. and Yildiz, M. (2025), "Evaluating the influence of service conditions on the out-of-plane and in-plane loading performance and damage behavior of unidirectional CFPEKK composites for aerospace applications", *Composites Part B: Engineering*, Vol. 304, 112637, doi: 10.1016/j.compositesb.2025.112637.

Zhang, S., Ma, D., Rezasefat, M., Amico, S. and Manes, A. (2025a), "Investigation on progressive damage evolution for low-velocity impact simulation of woven composites", *International Journal of Impact Engineering*, Vol. 202, 105316, doi: 10.1016/j.ijimpeng.2025.105316.

Zhang, Y., Guangshuo, F. and Bo, L. (2025b), "A machine learning-based prediction model for the impact mechanical response of composite laminates considering microstructure sensitive transverse properties", *Polymer Composites*, Vol. 46 No. 4, pp. 3742-3754, doi: 10.1002/pc.29203.

Corresponding author
Dayou Ma can be contacted at: dayou.ma@polimi.it

For instructions on how to order reprints of this article, please visit our website:
www.emeraldgrouppublishing.com/licensing/reprints.htm
Or contact us for further details: **permissions@emeraldinsight.com**

Downloaded from http://www.emerald.com/ijsi/article-pdf/doi/10.1108/IJSI-07-2025-0180/10416281/ijsi-07-2025-0180en.pdf by Politecnico di Milano user on 06 March 2026